ELSEVIER

Alkali metal-induced Si(1 1 1) $\sqrt{21} \times \sqrt{21}$ structure: The Na case

M. D'angelo [a],[*], M. Konishi [a], I. Matsuda [a], C. Liu [a], S. Hasegawa [a],
T. Okuda [b], T. Kinoshita [b]

[a] *Department of Physics, School of Science, The University of Tokyo, 7-3-1 Hongo, Bunkyo-ku, Tokyo 113-0033, Japan*
[b] *Synchrotron Radiation Laboratory, Institute for Solid State Physics, The University of Tokyo, 5-1-5 Kashiwanoha,
Kashiwa 277-8581, Japan*

Abstract

We report the first scanning tunneling microscopy (STM) and core-level photoemission (CL-PES) studies of a $\sqrt{21} \times \sqrt{21}$ structure induced by sub-monolayer Na deposition on the Si(1 1 1) $\sqrt{3} \times \sqrt{3}$-Ag surface. In the filled-state STM images, five bright protrusions in the $\sqrt{21} \times \sqrt{21}$ unit cell are located on the Ag trimers of the $\sqrt{3} \times \sqrt{3}$-Ag structure. The Si 2p core-level photoemission decomposition shows that the surface-shifted component originated from the Si-trimer atoms in the $\sqrt{3} \times \sqrt{3}$-Ag surface splits into two for the $\sqrt{21} \times \sqrt{21}$ structure, which are attributed to the Si-trimer atoms in the $\sqrt{21} \times \sqrt{21}$ unit cell which are affected and unaffected by the Na adsorption. These results show strong similarities between the Na-induced $\sqrt{21} \times \sqrt{21}$ superstructure and the noble metal-induced ones, indicating a common atomic structure and formation mechanism.
© 2005 Elsevier B.V. All rights reserved.

Keywords: Scanning tunneling microscopy; Photoelectron spectroscopy; Surface reconstructions; Silicon; Silver; Sodium

1. Introduction

Alkali metal or noble metals on semiconductor surfaces are model systems to study metal/semiconductor interaction because of the simple elec-

tronic structure of the adsorbates. Particularly, the $\sqrt{3} \times \sqrt{3}$-Ag superstructure induced by deposition of one monolayer (ML) of Ag atoms on the Si(1 1 1) surface is one of the most important prototypes for metal/semiconductor interfaces [1,2]. Further adsorption of monovalent atoms (alkali metals or noble metals) on the Ag-induced $\sqrt{3} \times \sqrt{3}$ surface leads to a $\sqrt{21} \times \sqrt{21}$ reconstruction. The noble metal-induced $\sqrt{21} \times \sqrt{21}$

---

superstructures have been widely studied with many different techniques such as reflection-high-energy electron diffraction (RHEED) [3], scanning tunneling microscopy (STM) [3,4], angle-resolved ultraviolet photoemission spectroscopy (ARUPS) [5–9], core-level photoemission spectroscopy (CL-PES) [10], and grazing-incidence X-ray diffraction (GIXRD) [11]. Transport measurements show high surface electrical conductivity due to electron transfer from the adatoms to the surface-state band of the $\sqrt{3} \times \sqrt{3}$-Ag surface [2,12]. For Ag, Au and Cu, the $\sqrt{21} \times \sqrt{21}$ phases show similar band structures and STM images, suggesting that the atomic structures for all noble metal-induced $\sqrt{21} \times \sqrt{21}$ superstructures are basically the same. However, the structure itself is still under debate with different models proposed involving 3, 4 or 5 adatoms per $\sqrt{21} \times \sqrt{21}$ unit cell [3–5,11]. Furthermore, in the case of alkali metal-induced $\sqrt{21} \times \sqrt{21}$ superstructures, only a few studies have been reported so far: an STM and a photoemission study on Cs adsorption [13], an angle-resolved valence band and core-level spectroscopy study of the Cs- and K-induced $\sqrt{21} \times \sqrt{21}$ phases [14] and conductivity measurements on K and Cs adsorption by macro-four point probes technique [2,15]. Interestingly, for the $\sqrt{21} \times \sqrt{21}$-(Ag, Cs) case, the situation looks more complicated than for noble-metal with electron diffraction observation revealing the existence of two kinds of $\sqrt{21} \times \sqrt{21}$ phases depending on the Cs-coverage. The high Cs-coverage $\sqrt{21} \times \sqrt{21}$ phase show quite different STM images and band structure compared to the noble metal-induced $\sqrt{21} \times \sqrt{21}$ phase, suggesting a different formation process. As emphasized in a recent review article [16], even simple metal/semiconductor interfaces can have complex behaviors and understanding them requires a deep insight of the system. In this view, further experiments on the alkali metal-induced $\sqrt{21} \times \sqrt{21}$ superstructures are needed. Indeed, having a unifying view for the noble-metal and alkali-metal induced reconstructions would allow a comprehensive understanding of the formation process and properties of the $\sqrt{21} \times \sqrt{21}$ phases. We have chosen the Na-induced $\sqrt{21} \times \sqrt{21}$ superstructure because Na is the most simple alkali metal atom which does not interdiffuse into Si

crystal. Besides, a recent ARUPS study [17] shows that, in contrast to the Cs case, the Na-induced $\sqrt{21} \times \sqrt{21}$ phase has a band structure similar to the noble-metal induced $\sqrt{21} \times \sqrt{21}$ superstructures. We report here the first study of the Na-induced $\sqrt{21} \times \sqrt{21}$ reconstruction by STM combined with Si 2p CL-PES analysis. The decomposition shows, at least, three surface-shifted components; two are attributed to the Si-trimer atoms and the third one is assigned to the Si atoms in the atomic plane below the Si trimers. The former two components are split from a single component of the $\sqrt{3} \times \sqrt{3}$-Ag structure because some of the Si trimers are affected by the Na adsorption and the others are not involved in the $\sqrt{21} \times \sqrt{21}$-(Ag, Na) phase. Both STM and CL-PES results show strong similarities with those obtained on the noble-metal-induced $\sqrt{21} \times \sqrt{21}$ phases. These results indicate a common structure and formation mechanism between the two surface superstructures.

2. Experimental details

The STM experiments were carried out on a commercial ultrahigh-vacuum low-temperature Unisoku STM (USM-501) equipped with a RHEED and evaporation sources. All the images shown here were taken at 65 K. The CL-PES measurements were performed on beam-line BL-18A (Institute of Solid State Physics, the University of Tokyo) at Photon Factory, in KEK, Japan, using a VG ADES 500 angle-resolved photoelectron spectrometer. The surface quality was checked by low-energy electron diffraction (LEED), Si 2p core-level and valence-band spectra. The base pressure during the STM and CL-PES experiments was better than 1×10^{-10} Torr. The sample crystal was a p-type Si(111) flat surface. Native oxides and impurities were removed in situ by sequences of resistive thermal annealing up to 1200 °C, leading to a clear 7×7 surface reconstruction. The Si(111)$\sqrt{3} \times \sqrt{3}$-Ag surface was then prepared by depositing 1 ML of Ag atoms on the substrate kept at ~500 °C. 1 ML corresponds to 7.83×10^{14} atom/cm^2, i.e. the density of Si atoms in the topmost layer of the (111) face. Silver was evaporated

from a graphite effusion cell. Finally, we evaporated Na atoms on the $\sqrt{3} \times \sqrt{3}$-Ag surface at low temperature (around 150 K) from a thoroughly out-gassed SAES-getter source. The Na coverage was calibrated by depositing Na on the clean 7×7 at room temperature with the appearance of the $\delta(7 \times 7)$ phase corresponding to 1 ML of Na [18].

3. Results and discussion

3.1. STM observations

Fig. 1(a) shows a 16 nm × 16 nm filled-states STM topograph of the $\sqrt{3} \times \sqrt{3}$-Ag surface after Na deposition. One can see bright areas separated by darker areas. The bright areas are not seen before the Na deposition under the same STM imaging conditions and thus correspond to a Na-induced reconstruction. At this bias ($V_t = 0.5$ V), the darker areas show the pattern

of the $\sqrt{3} \times \sqrt{3}$-Ag surface structure. However, as shown below, some Na clusters are actually adsorbed on these regions and are not visible at low bias voltages.

If we have a closer look at the bright regions (Fig. 1(b)), we see that the Na atoms are organized into a periodic structure. The unit cell of this periodic pattern is drawn in white. As the $\sqrt{3} \times \sqrt{3}$-Ag pattern is visible, it allows us to identify an unit cell of the Na-induced superstructure. The length of basis vectors is approximately 2.6 times the length of the $\sqrt{3}$ basis vectors and thus corresponds to a $\sqrt{21} \times \sqrt{21}$ periodicity. For a comparison, a close scan of the $\sqrt{21} \times \sqrt{21}$-Ag superstructure as given in Ref. [6] is shown in Fig. 1(c). From these two images, it is obvious that STM topographs for the Na- and Ag-induced $\sqrt{21} \times \sqrt{21}$ superstructures are similar to each other.

If we come back to Fig. 1(a), we see two domains rotated by 21.8° from each other, in agreement with LEED observations [17]. For the
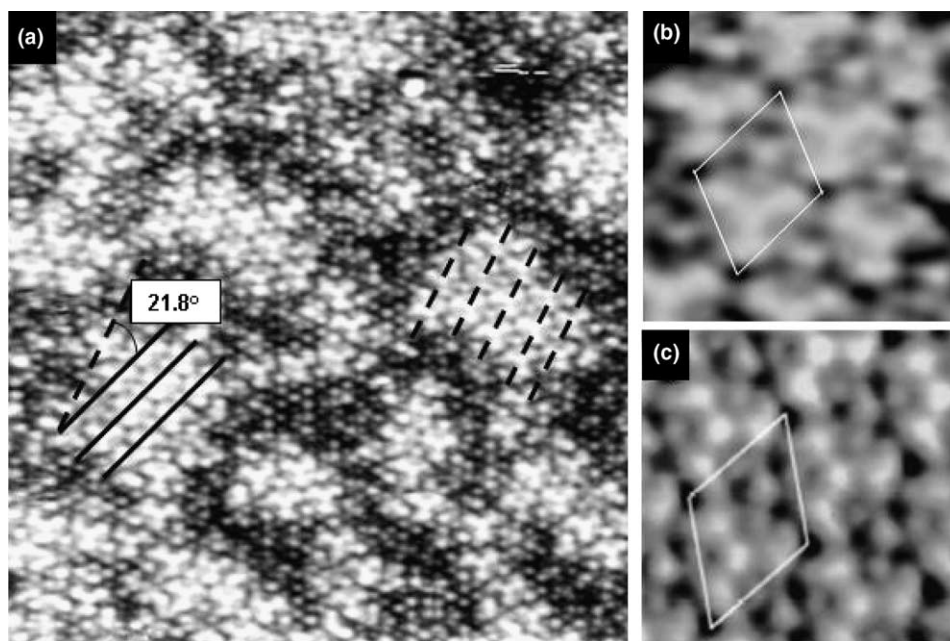

Fig. 1. STM topograph of the $\sqrt{21} \times \sqrt{21}$-(Ag, Na) surface. (a) 16 nm × 16 nm filled-state image with $V_t = 0.5$ V, $I_t = 0.5$ nA. Two domains are indicated by dashed and solid lines, which are rotated by 21.8° from each other. (b) Zoom on a $\sqrt{21} \times \sqrt{21}$-(Ag, Na) domain (2.6 nm × 2.6 nm filled-state image). The $\sqrt{21} \times \sqrt{21}$ unit cell is drawn in white. (c) For comparison, a filled-state image of the $\sqrt{21} \times \sqrt{21}$-Ag, with $V_t = 0.5$ V, $I_t = 0.35$ nA, as given by [6] (2.3 nm × 2.3 nm filled-state image).

Si(111)–$\sqrt{21} \times \sqrt{21}$-Ag superstructure, two domains are also reported [6], however, the domains are contiguous with straight domain boundaries and their size is larger than hundreds nanometers. In contrast, for the Na-induced $\sqrt{21} \times \sqrt{21}$ reconstruction, the domain size is a few nanometers at most, and no straight domain boundaries are observed.

We now turn to the bias dependence of STM images. Fig. 2 presents a series of 22 nm × 22 nm STM topographs of the same surface region taken at different bias voltages. Topographs (a)–(c) correspond to the filled-state images whereas images (d)–(f) correspond to the empty-state. On the topographs (a), (d) and (e) one can see bright regions of the $\sqrt{21} \times \sqrt{21}$-(Ag, Na) phase, but the aspect changes a lot with the tip bias, showing that the images are sensitive to the electronic structure. The bias dependence of the images as shown in Fig. 2(a), (b), (d) and (e) is similar to that for the $\sqrt{21} \times \sqrt{21}$-Ag surface reconstruction [6]. Interestingly, for higher bias voltages (typically 2 volts), the aspect of the topographs changes dramatically as seen in Fig. 2(c) and (f). The contrast is reversed and the $\sqrt{21} \times \sqrt{21}$-(Ag, Na) domains are no more visible. Instead, we can observe some bright protrusions of similar sizes randomly distributed. If we compare the STM topographs at low and high biases, we can see that these bright protrusions are located between the $\sqrt{21} \times \sqrt{21}$-(Ag, Na) domains. These protrusions are not visible on the clean Si(111)$\sqrt{3} \times \sqrt{3}$-Ag surface, and we have checked that their density increases with Na coverage (not shown here). Therefore, these features correspond to Na atoms. The typical size of these protrusions is 8 nm, indicating that one bright spot corresponds indeed to some tens of Na atoms, i.e. an Na cluster. Besides, a detailed analysis of the STM topographs shows that the protrusions have no special adsorption sites, in agreement with cluster formation and weak adsorbate/substrate interaction. At low positive and negative biases (typically between −1 and +1 V) these protrusions are not observable, as in Fig. 1, suggesting a semiconducting character of the clusters. Since the protrusions are visible only at high bias voltages ($|V_t| \geqslant 1$ V), they do not contribute to the density of states near the Fermi level. The

band structure within 1 eV below the Fermi level thus reflects the contribution from the $\sqrt{21} \times \sqrt{21}$ region only. Similar STM topograph between the $\sqrt{21} \times \sqrt{21}$-Ag and $\sqrt{21} \times \sqrt{21}$-(Ag, Na) surfaces is consistent with similar band structures as observed in the recent photoemission spectroscopy [17].

At this point, we would like to emphasize that the STM topographs we show here correspond to an optimal Na coverage for formation of the $\sqrt{21} \times \sqrt{21}$ phase. Indeed, Fig. 3 shows STM images (in the filled states) of the $\sqrt{3} \times \sqrt{3}$-Ag surface with different Na coverages. For low coverages (Fig. 3(a)), one can still see $\sqrt{3} \times \sqrt{3}$-Ag pattern and some bright spots corresponding to Na atoms. The Na atoms form clusters having specific shape. The shape of these feature is the same as the shape of Ag clusters observed on $\sqrt{3} \times \sqrt{3}$-Ag and called "propellers" [19]. So in the following text we also call the Na cluster having this specific shape a "propeller" (see also Fig. 4(a)). No $\sqrt{21} \times \sqrt{21}$ is visible yet at this coverage. Around 0.2 ML (Fig. 3(b)), the proportion of surface area covered by the $\sqrt{21} \times \sqrt{21}$ domains is optimum, but yet we can see that the domains are still small and separated by dark regions. For higher coverages (0.4 ML in Fig. 3(c)), the $\sqrt{21} \times \sqrt{21}$ structure is perturbed; the domain size is drastically reduced, and three-dimensional islands start to form all over the surface while the $\sqrt{3} \times \sqrt{3}$-Ag reconstruction is visible in between. For a clearer view, a zoom is provided on Fig. 3(c) in the insert. On this zoom, we can clearly see the $\sqrt{3} \times \sqrt{3}$-Ag substrate between the Na clusters. At further higher coverages, only the islands are visible (0.75 ML in Fig. 3(d)). Note that the islands formed at higher coverages are different in size and size distribution from the clusters observed at domain boundary regions at lower coverages seen in Fig. 2(c) and (f).

In order to have a better understanding of the Si(111) $\sqrt{21} \times \sqrt{21}$-(Ag, Na) reconstruction, we now look at a more detailed STM topograph (filled states) as shown in Fig. 4(a). In the center of this image, three propellers P1, P2 and P3 are aligned. These propellers are organized locally with a $\sqrt{21} \times \sqrt{21}$ periodicity. Interestingly, at this bias, the surrounding $\sqrt{3} \times \sqrt{3}$-Ag structure is visible
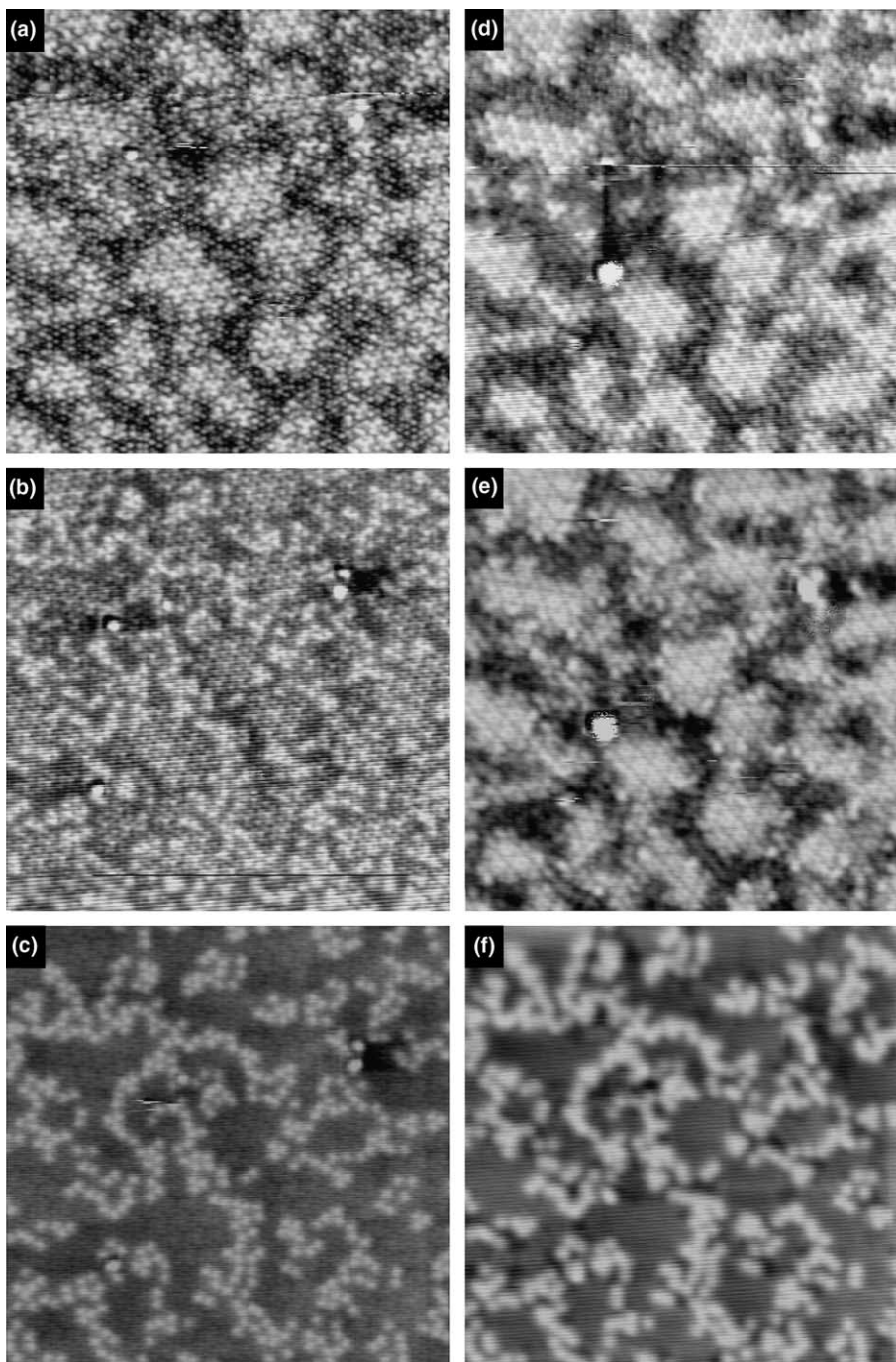
Fig. 2. A series of 22 nm × 22 nm STM topographs of the same region in the $\sqrt{21} \times \sqrt{21}$-(Ag, Na) phase, taken at 65 K for different bias voltages. Filled-state images: (a) $V_t = 0.5$ V, $I_t = 0.5$ nA; (b) $V_t = 1$ V, $I_t = 0.5$ nA; (c) $V_t = 2$ V, $I_t = 0.5$ nA. Empty-state images: (d) $V_t = -0.5$ V, $I_t = 0.5$ nA; (e) $V_t = -1$ V, $I_t = 0.5$ nA; (f) $V_t = -2$ V, $I_t = 0.5$ nA.

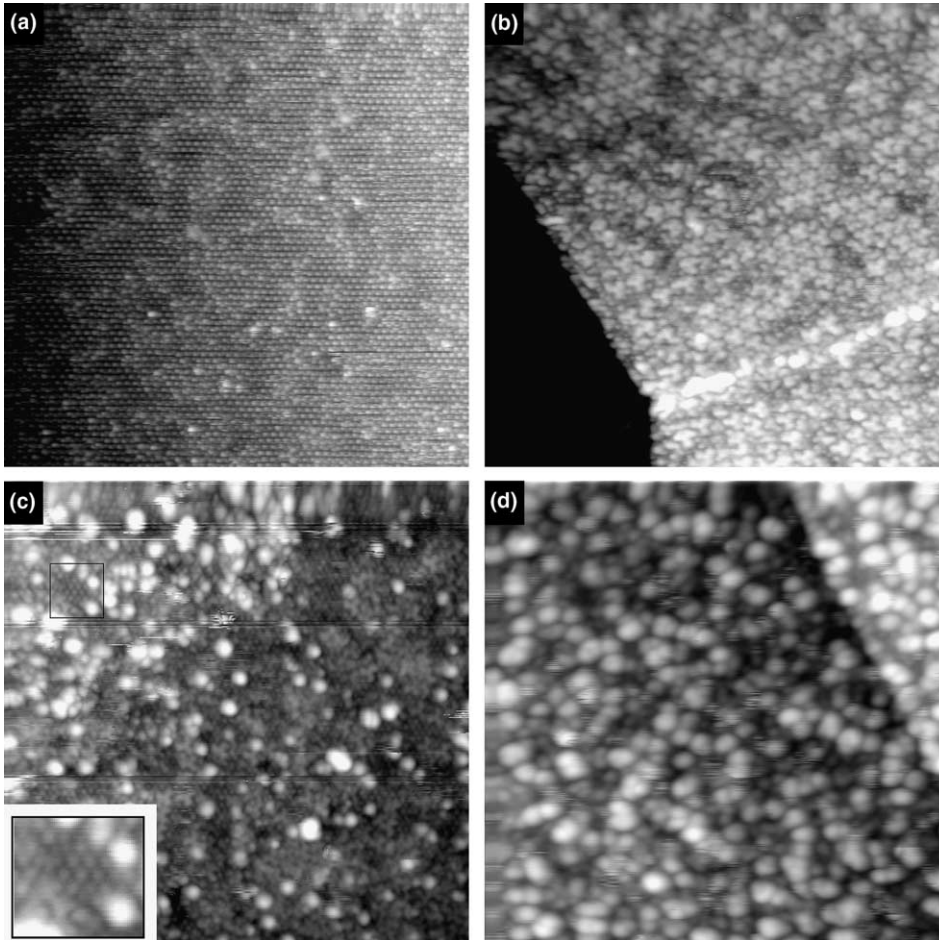Fig. 3. 16 nm × 16 nm Filled-state ($V_t = 0.5$ V, $I_t = 0.5$ nA) STM topographs of the Si(1 1 1)$\sqrt{3} \times \sqrt{3}$-Ag surface with deposition of different Na coverages. (a) 0.07 ML, (b) 0.2 ML, (c) 0.4 ML, and (d) 0.75 ML.

which allows us to analyze the $\sqrt{21} \times \sqrt{21}$ structure. We superimpose a mesh on the STM topograph, corresponding to the $\sqrt{3} \times \sqrt{3}$ periodicity (Fig. 4(b)). The $\sqrt{3} \times \sqrt{3}$-Ag structure model with the corresponding mesh is shown in Fig. 4 (lower left part). This model corresponds to the IET (Inequivalent Triangles) structure [1,20]: we have two Ag trimers per $\sqrt{3} \times \sqrt{3}$ unit cell which are slightly rotated one to the other and which are not equivalent in size (large Ag trimers and small Ag trimers). The grid intersections of our mesh correspond to the position of the bright spots visible in the STM topograph of the $\sqrt{3} \times \sqrt{3}$-Ag surface at a bias of 0.5 V, which correspond to the center of

Ag trimers (see the structure model of the $\sqrt{3} \times \sqrt{3}$-Ag surface at the lower left in Fig. 4). For more clarity, we give a schematic view of the STM image in Fig. 4(c). Five protrusions denoted by A, B, C, D and E are visible in the $\sqrt{21} \times \sqrt{21}$ unit cell. The bright spot named E is located at an intersection of the grid, that is to say on an Ag trimer. The protrusions A, B, C and D, which constitute the "propeller", are located in the center of triangles of the grid. Notice that there are two types of triangles in the grid, one directed to the left (noted L on the figure) and another to the right (noted R on the figure), corresponding to either Si trimers or larger Ag trimers (see the structure
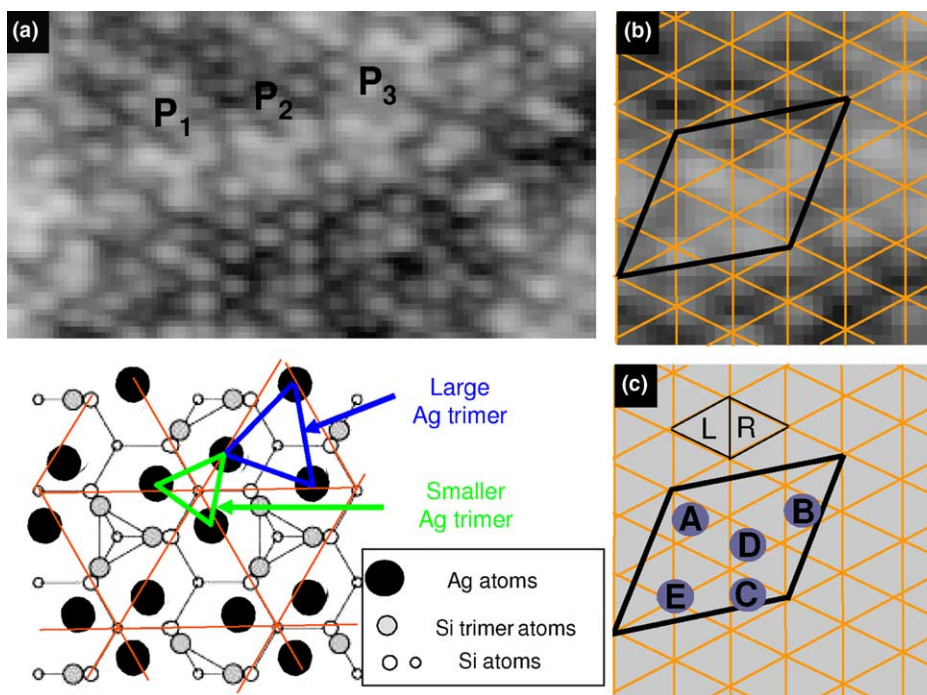
Fig. 4. (a) A 9 nm × 5 nm filled-state STM topograph of three Na propellers showing locally the $\sqrt{21} \times \sqrt{21}$ periodicity. The Na coverage is 0.2 ML. $V_t = 0.5$ V, $I_t = 0.5$ nA. At this bias, the surrounding $\sqrt{3} \times \sqrt{3}$-Ag domains are visible. (b) Zoom around one $\sqrt{21} \times \sqrt{21}$ unit cell. The mesh drawn on the STM image corresponds to the $\sqrt{3} \times \sqrt{3}$-Ag periodicity with the intersection of the grid corresponding to the position of the Ag trimers (visible as bright spots in the STM image). The atomic structure of the $\sqrt{3} \times \sqrt{3}$-Ag surface is drawn in the lower left. (c) Schematic view of the STM image. A, B, C, D and E correspond to the bright spots observed in the $\sqrt{21} \times \sqrt{21}$ unit cell.

model of the $\sqrt{3} \times \sqrt{3}$-Ag surface). The protrusions A, B, C, and D are all located on the same type of triangles (R triangles), i.e., they are all located either on Si trimers or Ag trimers. First-principle calculation shows, on the other hand, that adsorption of noble metal atoms on the $\sqrt{3} \times \sqrt{3}$-Ag surface is energetically favored on the Ag trimers rather than on the Si trimers [21]. Ag 4d peak width analysis with increasing Na deposition also suggests that adatoms are adsorbed on the Ag trimers of the $\sqrt{3} \times \sqrt{3}$ surface [17]. Thus, we propose that all protrusions A–E observed in the $\sqrt{21} \times \sqrt{21}$ image are located on Ag trimers. However, one should be careful when analyzing STM topographs, as the STM tip in the constant current mode follows the density-of-state contours. Thus, at this stage it is not possible to say if one bright protrusion corresponds to a Na atom or is due to an electronic effect.

Indeed, in the case of noble-metal adsorption, no consensus has been achieved so far for the structure of the $\sqrt{21} \times \sqrt{21}$ reconstructions and several different models have been proposed involving 3, 4 or 5 adatoms per $\sqrt{21} \times \sqrt{21}$ unit cell [4,3,11,5,21]. At least we can affirm that the location of the bright spots in our STM topographs of the Si(1 1 1)$\sqrt{21} \times \sqrt{21}$-(Ag, Na) surface correspond to the position of the bright spots on the Si(1 1 1)$\sqrt{21} \times \sqrt{21}$-(Ag, Au) as observed by Nogami et al. with five bright spots per unit cell all located on Ag trimers.

3.2. Photoemission measurements

To study more carefully the similarities between the Si(1 1 1)$\sqrt{21} \times \sqrt{21}$-Ag and the Si(1 1 1)$\sqrt{21} \times \sqrt{21}$-(Ag, Na) superstructures, we now look at
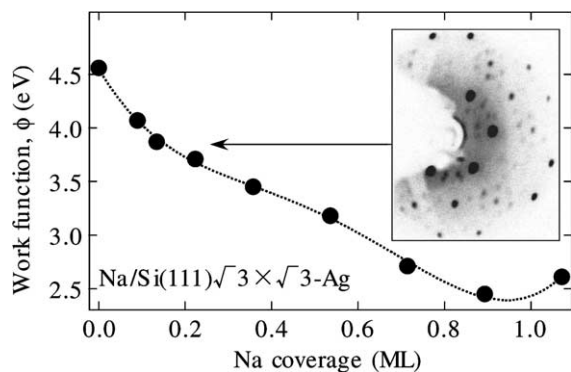
Fig. 5. Change in work function induced by Na deposition on the $\sqrt{3} \times \sqrt{3}$-Ag surface at 130 K.

photoemission results and more particularly at the Si 2p CL-PES for these two surfaces.

Fig. 5 displays the change in work function with increasing Na deposition on the $\sqrt{3} \times \sqrt{3}$-Ag surface at 130 K. The value of the work function was obtained by the total energy width of the spectra from secondary electron cut-off to the Fermi level. The Na coverage is calibrated through comparisons of the normalized Na 2s photoemission intensity as well as the core-level emission intensity ratio Na 2s/Si 3p with that of the $\delta(7 \times 7)$ phase corresponding to 1 ML Na deposition on the clean 7×7 surface at room temperature [22]. The work function decreases with Na deposition and has a minimum of 2.4 eV around 1 ML coverage. As seen on Fig. 5, the work function does not decrease in a monotonous way, but rather stepwise. First, the work function decreases quite rapidly up to a coverage around 0.13–0.22 ML. This coverage range corresponds to the appearance of a clear $\sqrt{21} \times \sqrt{21}$-(LEED) pattern (see inset in Fig. 5). As seen from the STM images, it corresponds to the optimal Na coverage for the $\sqrt{21} \times \sqrt{21}$ surface. For higher Na coverages, the work function still decreases and reaches a minimum of 2.4 eV around 1 ML. This minimum value compares well with 2.36 eV, the work function value for polycrystalline Na [23]. This can be correlated to the STM observations showing that the surface is covered with Na islands for Na coverages around 1 ML (see Fig. 3(d)). It is also interesting to compare

this work function change with that obtained for the $\sqrt{21} \times \sqrt{21}$-Ag surface. In this case, for a Ag coverage around 0.15–0.2 ML, corresponding to the formation of $\sqrt{21} \times \sqrt{21}$ phase, the work function change is about −0.4 eV, which is to be compared with −0.7 eV for the Na-induced $\sqrt{21} \times \sqrt{21}$ phase at the same coverage. The work function change for semiconductors, in general, contains two contributions, the change in band bending and a surface dipole contribution [24]. For the $\sqrt{21} \times \sqrt{21}$-Ag case, the band bending change upon Ag deposition, which was measured by Si 2p core-level shifts, was about −0.4 eV, implying that the dipole contribution to the work function change is negligible. On the other hand, for the Na-induced $\sqrt{21} \times \sqrt{21}$ case, the band bending change upon Na deposition is also around −0.4 eV, so that the dipole contribution is around 0.3 eV, which is not negligible. We attribute this difference between the Ag- and Na-induced $\sqrt{21} \times \sqrt{21}$ phases to the contribution of Na clusters in the dark domains coexisting with the $\sqrt{21} \times \sqrt{21}$ domains, whose formation was evidenced by STM in Figs. 1 and 2.

Fig. 6 displays the Si 2p spectra for the $\sqrt{3} \times \sqrt{3}$-Ag (Fig. 6(a) and (b)), $\sqrt{21} \times \sqrt{21}$-Ag (Fig. 6(c) and (d)), and $\sqrt{21} \times \sqrt{21}$-(Ag, Na) (Fig. 6 (e) and (f)) surfaces, after background subtraction. The incident photon energy was 134 eV. For each reconstruction, we show two spectra, one corresponding to a bulk sensitive regime (at the photon incidence angle of $\theta_e = 0°$, (a), (c), and (e)) and another to a surface sensitive regime ($\theta_e = 60°$, (b), (d), and (f)). We proceed to peak decomposition using a least-square fitting method. The results are shown in Fig. 6. Each spectrum is decomposed using Voigt or Doniach-Sunjic functions with a spin-orbit splitting of 602 meV and a 85 meV Lorentzian width.

The decomposition of Si 2p core-level spectra for the Si(111)$\sqrt{3} \times \sqrt{3}$-Ag surface shows three major components (see Fig. 6(a) and (b)): one bulk component (B) and two surface-shifted components noted α and β. The binding energy of each surface-shifted component with respect to the bulk component obtained after the fitting procedure are summarized in Table 1. The α and β components correspond to the Si-trimer atoms and the second
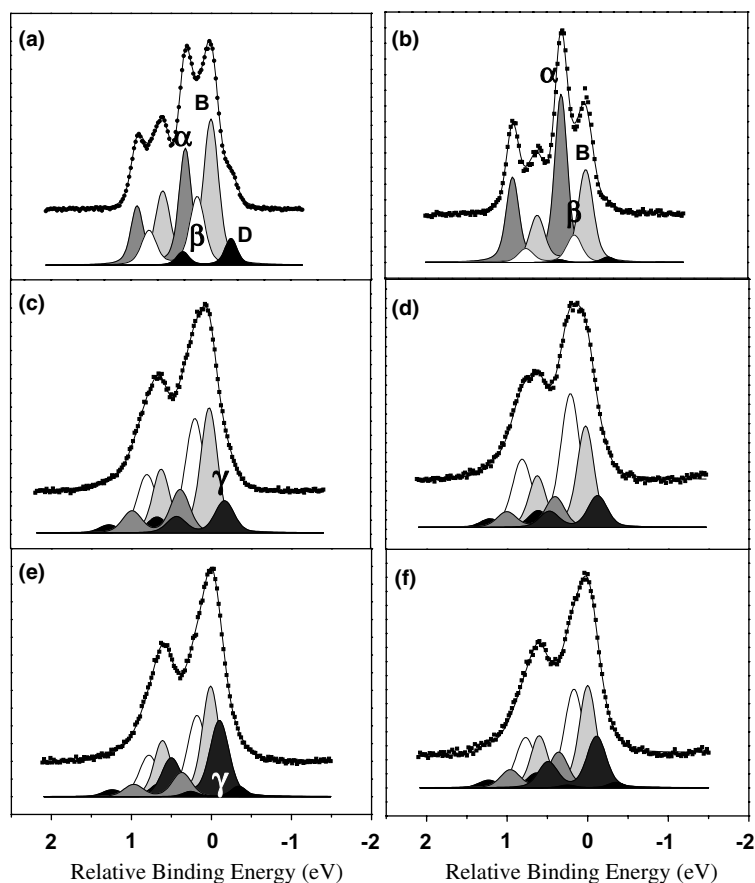
Fig. 6. Si 2p core-level photoemission spectra. The incident photon energy was 134 eV. The spectra correspond to the following superstructures: Si(111)$\sqrt{3} \times \sqrt{3}$-Ag: (a) $\theta = 0°$, (b) $\theta = 60°$. Si(111)$\sqrt{21} \times \sqrt{21}$-Ag: (c) $\theta = 0°$, (d) $\theta = 60°$. Si(111)$\sqrt{21} \times \sqrt{21}$-(Ag, Na): (e) and $\theta = 0°$, (f) $\theta = 60°$.

layer Si atoms respectively, according to the previous studies [10,25,26]. The small component of lower binding energy, noted D, is attributed to defects on the $\sqrt{3} \times \sqrt{3}$-Ag surface [26]. If we now look at Fig. 6(c) and (d), the Si 2p core-level decomposition for the Si(111)$\sqrt{21} \times \sqrt{21}$-Ag superstructure shows at least three surface-shifted components, α, β, and γ, whose binding energies relative to the bulk component B are 0.38, 0.19 and −0.15 eV, respectively (see Table 1). The higher binding-energy components at 0.38 and 0.19 eV have energy shifts similar to those of the α and β components of the $\sqrt{3} \times \sqrt{3}$-Ag surface, and then are attributed to the Si-trimer atoms and the second Si layer atoms, respectively. The lower binding-energy component at −0.15 eV (noted γ) is

Table 1
Relative binding energy of the surface-shifted components for the different superstructures

Compo-nents	Energy shift (eV)		
	$\sqrt{3} \times \sqrt{3}$-Ag	$\sqrt{21} \times \sqrt{21}$-Ag	$\sqrt{21} \times \sqrt{21}$-Na
B	0	0	0
α	0.31	0.38	0.36
β	0.16	0.19	0.17
γ	/	−0.15	−0.11

believed to derive from the α component assigned to the Si trimers of the $\sqrt{3} \times \sqrt{3}$-Ag. For the $\sqrt{3} \times \sqrt{3}$-Ag superstructure, all Si-trimer atoms are equivalent because all the Si atoms bond to

Ag atoms. However, since the $\sqrt{21} \times \sqrt{21}$-Ag superstructure is prepared by additional Ag deposition on the $\sqrt{3} \times \sqrt{3}$-Ag surface, these additional Ag atoms adsorb on some Ag trimers of the $\sqrt{3} \times \sqrt{3}$-Ag surface. Thus, in the $\sqrt{21} \times \sqrt{21}$-Ag structure, all Si trimers are not equivalent; some Si trimers are bounded to Ag trimers on which an additional Ag atom is adsorbed ("affected" Si-trimer atoms) and other Si trimers are connected to Ag trimers on which no additional Ag atom is adsorbed ("unaffected" Si-trimer atoms). This inequivalent electronic environment for the Si trimers gives rise to a new component in the Si 2p core-level decomposition, the γ component assigned to the "affected" Si-trimer atoms. Note that the γ component has a more electron rich environment and thus a lower binding energy than the α component, in agreement with charge transfer from the additional Ag atom to the substrate.

In case of the Na-induced $\sqrt{21} \times \sqrt{21}$ superstructure in Fig. 6(e) and (f), Si 2p core-level emission analysis shows also three surface-shifted components. The relative binding energies are 0.36, 0.17 and −0.11 eV for α, β and γ components, respectively. These values are very close to those obtained in the above-mentioned $\sqrt{21} \times \sqrt{21}$-Ag case. Thus, we can also assign the α component to the "unaffected" Si-trimer atoms, β to the second-layer Si atoms, and γ to the "affected" Si-trimer atoms. So, in agreement with quite similar STM images for the $\sqrt{21} \times \sqrt{21}$-Ag and $\sqrt{21} \times \sqrt{21}$-(Ag, Na) superstructures (Fig. 1), the Si 2p core-level spectra also present strong similarities. However, a slight difference in relative intensity among the components can be noticed. Particularly, the γ component has higher intensity than α on the Na-induced $\sqrt{21}$ phase whereas it has lower intensity for the $\sqrt{21} \times \sqrt{21}$-Ag surface. This suggests a higher number of "affected" Si-trimers in the Na case, which may result from the presence of Na clusters in the dark domains evidenced by STM (see Figs. 1 and 2). Finally, we briefly comment on the intensity of the β component which appears to be higher for both the Ag- and Na-induced $\sqrt{21} \times \sqrt{21}$ superstructures than for the $\sqrt{3} \times \sqrt{3}$ surface. This can be explained in terms of photodiffraction effect. Another possible explanation can be that the β component has

more than one contribution on the $\sqrt{21} \times \sqrt{21}$ surface coming from the "affected" Si trimers.

4. Conclusion

We have investigated the $\sqrt{21} \times \sqrt{21}$-(Ag, Na) superstructure by STM and core-level photoemission spectroscopy, together with the $\sqrt{21} \times \sqrt{21}$-Ag superstructure for comparison. In contrast to the Cs-induced $\sqrt{21} \times \sqrt{21}$ surface studied so far, the STM images of the Na-induced one show strong similarities with the $\sqrt{21} \times \sqrt{21}$ surface induced by noble metals adsorption in STM appearance and Si 2p core-level states. The only difference is that the domains of the $\sqrt{21} \times \sqrt{21}$-(Ag, Na) structure are much smaller than those of the Ag-induced one, and they are separated by thin domains containing randomly adsorbed Na clusters. The Si 2p core-level photoemission from $\sqrt{21} \times \sqrt{21}$-(Ag, Na) shows three surface-shifted components, which are assigned to contributions from Si atoms in the atomic plane below the Si trimers, affected and unaffected Si-trimer atoms, respectively. This decomposition is identical to that obtained for the $\sqrt{21} \times \sqrt{21}$-Ag superstructure. These results suggest a similar atomic structure for the $\sqrt{21} \times \sqrt{21}$-Ag and $\sqrt{21} \times \sqrt{21}$-(Ag, Na) phases.

References

[1] I. Matsuda, H. Morikawa, C. Liu, S. Ohuchi, S. Hasegawa, T. Okuda, T. Kinoshita, C. Ottaviani, A. Cricenti, M. D'angelo, P. Soukiassian, G. Le Lay, Phys. Rev. B 68 (2003) 085407.

[2] S. Hasegawa, X. Tomg, S. Takeda, N. Sato, T. Nagao, Prog. Surf. Sci. 60 (1999) 89.

[3] A. Ichimiya, H. Nomura, Y. Horio, Surf. Rev. Lett. 1 (1994) 1.

[4] J. Nogami, K.J. Wan, X.F. Lin, Surf. Sci. 306 (1994) 81.

[5] X. Tong, Y. Sugiura, T. Nagao, T. Takami, S. Takeda, S. Ino, S. Hasegawa, Surf. Sci. 408 (1998) 146.

[6] X. Tong, S. Ohuchi, N. Sato, T. Tanikawa, T. Nagao, I. Matsuda, Y. Aoyagi, S. Hasegawa, Phys. Rev. B 64 (2001) 205316.

[7] H.M. Zhang, K. Sakamoto, R.I.G. Uhrberg, Phys. Rev. B 64 (2001) 245421. Appl. Surf. Sci. 190, 103 (2002).

[8] J.N. Crain, K.N. Altmann, C. Bromberger, F.J. Himpsel, Phys. Rev. B 66 (2002) 205302.

[9] X. Tong, C.S. Jiang, S. Hasegawa, Phys. Rev. B 57 (1998) 9015.

[10] X. Tong, S. Ohuchi, T. Tanikawa, A. Harasawa, T. Okuda, Y. Aoyagi, T. Kinoshita, S. Hasegawa, Appl. Surf. Sci. 190 (2002) 121.

[11] H. Tajiri, K. Sumitani, W. Yashiro, S. Nakatani, T. Takahashi, K. Akimoto, H. Sugiyama, X. Zhang, H. Kawata, Surf. Sci. 493 (2001) 214.

[12] S. Hasegawa, X. Tong, C.-S. Jiang, Y. Nakajima, T. Nagao, Surf. Sci. 386 (1997) 322.

[13] C. Liu, I. Matsuda, H. Morikawa, H. Okino, T. Okuda, T. Kinoshita, S. Hasegawa, Jpn. J. Appl. Phys. 42 (2003) 1659.

[14] H.M. Zhang, K. Sakamoto, R.I.G. Uhrberg, Phys. Rev. B 70 (2004) 245301.

[15] S. Hasegawa, K. Tsuchie, K. Toriyama, X. Tong, T. Nagao, Appl. Surf. Sci. 162–163 (2000) 42.

[16] M.E. Davila, J. Avila, M.C. Asencio, G. Le Lay, Surf. Rev. Lett. 10 (2003) 981.

[17] M. Konishi, I. Matsuda, C. Liu, H. Morikawa, S. Hasegawa, T. Okuda, T. Kinoshita, J. Surf. Sci. Nanotech. 3 (2005) 107;
I. Matsuda, T. Hirahara, M. Konishi, C. Liu, H. Morikawa, M. D'angelo, S. Hasegawa, T. Okuda, T. Kinoshita, Phys. Rev. B 71 (2005) 235315.

[18] J.J. Paggel, G. Neuhold, H. Haak, K. Horn, Surf. Sci. 414 (1998) 221.

[19] N. Sato, T. Nagao, S. Hasegawa, Phys. Rev. B 60 (1999) 16083.

[20] H. Aizawa, M. Tsukada, N. Sato, S. Hasegawa, Surf. Sci. 429 (1999) L509.

[21] H. Aizawa, M. Tsukada, Phys. Rev. B 59 (1999) 10923.

[22] T. Okuda, H. Shigeoka, H. Daimon, S. Suga, T. Kinoshita, A. Kakizaki, Surf. Sci. 321 (1994) 105.

[23] S. Hüfner, Photoelectron Spectroscopy, in: Springer series in solid-state sciences, vol. 82, 1996.

[24] H. Luth, Surfaces and Interfaces of Solids, in: Springer series in solid-state sciences, vol. 15, 1993, p. 499.

[25] G. Le Lay, M. Göthelid, A. Cricenti, C. Håkansson, P. Perfetti, Europhys. Lett. 45 (1998) 65.

[26] R.I.G. Uhrberg, H.M. Zhang, T. Balasubramanian, E. Landemark, H.W. Yeom, Phys. Rev. B 65 (2002) 081305R.